STABLE CRACK GROWTH STUDY ON A MODEL GEOMETRY

P.A.J.M. Steenkamp*

Conformity of J-controlled crack initiation and growth behaviour for specimens and structural geometries forms a key assumption underlying J-based fracture safety assessment procedures. The present paper investigates the validity of this assumption for a specific material, A387 Gr.D, and model geometry by a combined experimental/numerical study. Good agreement is found between structural and specimen crack growth behaviour in terms of J-R curves, provided that the effects of crack tip constraint and orientation with respect to the rolling direction are taken into account.

INTRODUCTION

The potentially catastrophic consequences of failure by fracture of heavy section steel structures such as e.g. nuclear and chemical pressure vessels and offshore platforms due to the presence of cracks has led to extensive research in the field of (Linear-Elastic and Elastic-Plastic) Fracture Mechanics over the past decades. In many instances the high fracture toughness at operating temperature of pressure vessel steels leads to the formation of large plastic zones in the cracked area prior to crack extension, thus invalidating the LEFM approach and necessitating EPFM methods. These methods, originally developed for the prediction of crack extension initiation under elastic-plastic conditions, are being extended to describe the stable crack growth characteristics of ductile pressure vessel steels, where fracture toughness usually rises significantly as the load is increased beyond crack extension initiation. This effect represents an important margin of safety against final instability of a cracked structure.

* Formerly: Laboratory for Thermal Power Engineering, Delft University of Technology, Delft, The Netherlands. Presently with Shell Internationale Petroleum Maatschappij, The Hague, The Netherlands.

The key assumption underlying fracture safety assessments based on the J-integral is the conformity of J-controlled crack initiation and growth behaviour for two-dimensional specimens and three-dimensional structural geometries. Demonstration of the validity of this assumption requires direct comparisons between specimen- and structural J-R curve behaviour. Due to their cost and complexity, few such demonstrations have been published to date. In this paper J-R curves obtained from Single Edge Notched Bend (SENB) specimens are compared to J-R curves obtained on plate models with corner cracks emanating from a central hole. The procedure for obtaining the latter group of J-R curves is outlined in figure 1. After testing the model and severing the remaining surrounding ligament by fatigue cycling, crack extension was measured along the crack front. Combination of this crack growth distribution with the computed J-distribution, determined from an elastic-plastic finite element analysis of the geometry under consideration, yielded the J-R curve for the model. The results presented in this paper are more extensively discussed in Steenkamp (1).

EXPERIMENTS

Material and Geometries

All specimens and models used in this study were cut from the same 65 mm thick A387 Gr.D (2.25 Cr1Mo) steel plate, for which the engineering stress-strain data are given in figure 2. This figure also gives the dimensions of the plate models as well as the location and orientation of the specimen coupons. In addition to 25 mm thick standard-sized plane sided and 20% side grooved SENB specimens (width 50 mm, span 200 mm) with cracks either in the TS or in the TL direction, a few thinner (5 mm thick) plane sided specimens with in-plane dimensions identical to those of the standard specimens were also machined (TS orientation only), resulting in five groups of specimens. All specimens and plate models were precracked by spark erosion.

Specimen Experiments

Single specimen J-R curves were obtained for all specimens using the dye penetrant procedure described in Steenkamp (1) and Steenkamp & Hartevelt (2). Use was made of the modified-J concept by Ernst (3) as the crack was extended up to about 30% of the original specimen ligament. For each group of specimens, a mean curve was determined from the individual resistance curves using the least-squares method. These resulting curves are given in figure 3, from which it is seen that:

* this material heat exhibits a larger resistance to crack extension in the plate thickness direction (TS) than in the plate width direction (TL);
* consistent with observations reported elsewhere, J-R curves for plane sided specimens are much higher than those obtained from side grooved specimens. For the latter specimens, no appreciable through-thickness contraction was observed, and hence full plane strain constraint may be assumed for these specimens;
* the J-R curves obtained from the thin specimens are much higher than those obtained from thicker specimens of identical geometry and orientation, as the stress state in the thin specimens approaches plane stress conditions.

From the above observations it may be concluded that the upper and lower bound J-R curves for this material heat are given in figure 3 by the 5 mm thick, plane sided TS and the 25 mm thick side grooved TL curves, respectively.

Model Experiments

Two plate models were subsequently tested by uniaxial, displacement controlled loading. Several times during the loading, the testing was interrupted for dye penetrant marking of the crack front. By this procedure, a total of seven beach marks were obtained from the two model plates. The seven crack growth distributions along the crack front, determined in each case by averaging the results of the two corner cracks per model, are given in figure 4.

FINITE ELEMENT ANALYSES

Modeling

Several three-dimensional (infinitesimal strains) elastic-plastic finite element analyses were performed using the MARC program. For symmetry reasons only one-quarter of the plate was modeled. At first a mesh with four elements along the crack front was used. When the first computational results indicated the need for more refined meshes, a second mesh with six elements along the crack front was developed. Details of these meshes, subsequently referred to as a4 and a6, respectively, are given in table 1 and figure 5. The crack tip brick elements are collapsed to wedges with independent crack tip nodes, introducing a 1/r singularity in the crack tip strains. Elements with a reduced 2x2x2 Gaussian integration scheme were used in all cases. For details on the finite element solution procedures the reader is referred to Bakker (4). Each finite element model was loaded by stepwise increases of the uniform end displacement applied at a distance of 400 mm from the crack plane (cf. figure 5), equivalent to half the gage length of the LVDT's used in the experiments (cf. figure 2).

TABLE 1 - Details of the finite element meshes for the plate model geometries.

	a4	a6
type of elements	20 node brick, isoparametric, red. int.	
number of elements	159	222
number of nodes	864	1191
degrees of freedom	2451	3368
CPU-time ratio	1.00	1.99

Computational Results

The a6 finite element computation consisted of one elastic increment (#1), followed by 13 elastic-plastic displacement increments (#2-14), all indicated by number in figure 6, where the computed load-displacement curve is seen to compare well with the model's experimentally observed behaviour. This increment numbering (with accompanying displacement levels) will be maintained throughout the remainder of this paper. (The a4 computation was performed up to increment 10 only).

The spreading of the plastic zone in the plate with increasing load is shown in figure 7. Crack extension initiation in the experiments is assumed to have occurred at $\Delta \approx 1.5$ mm (cf. Steenkamp (1)), i.e. between increments 7 and 8 and hence in a state of contained yield, well below limit load.

The J-values at the nodal points along the crack front were determined for each increment by the virtual crack extension technique, using the post-processor VIRTUAL, Bakker (4). The path independence of J was verified by computing J for four concentric paths surrounding the crack tip.

The elastic-plastic J-distributions along the crack front for the a6 and a4 analyses are given in figure 8 by the solid and dashed lines, respectively. The J-values for the interior part of the crack front are seen to increase markedly with the displacement, with increasingly steep decreases near the stress-free surfaces. These observations are in accordance with similar results reported by e.g. Bakker (4) and De Lorenzi & Shih (5). The J-values near the central hole ($\phi \approx 90°$) are higher than those near the plate's free surface ($\phi \approx 0°$), which is attributed to the increasingly steep stress gradient near the hole.The two sets of results (viz. for the a4 and a6 analyses) nearly coincide for the initial increments, but deviate from each other with increasing plasticity, indicating the inability of the coarse a4 mesh to properly model the increasingly steeper gradients in the J-distribution along the crack front.

The local degree of plane strain constraint along the crack front can be defined by the constraint factor ν_c:

$$\nu_c = \frac{\sigma_z'}{\sigma_x' + \sigma_y'} \qquad (1)$$

where σ_x', σ_y' and σ_z' are the orthogonal, tensile stresses in a local coordinate system, with the z'-axis parallel to the local crack front. Figure 9 gives the ν_c distributions along the crack front of the plate models (the local stresses from which ν_c is computed are defined by the insert). For plane stress conditions, $\sigma_z' = 0$ and hence $\nu_c' = 0$; while for plane strain, ν_c will equal ν (= Poisson's ratio) for linear elastic and 0.5 for fully plastic conditions, respectively. From figure 9 it is seen that the crack tip constraint for the plate model remains well below the plane strain values in both the elastic and (fully) plastic cases. The significance of this observation will follow from the discussion in the next section.

COMPARISON BETWEEN SPECIMENS AND MODELS

Application of the procedure outlined in figure 1, viz. combining the computed J data from figure 8 (a6 analysis) and the experimentally obtained beach mark Δa-values from figure 4 for any angle ϕ along the crack front, yields the model's local J-R curves (i.e. J-R curves specific to the various positions locally along the crack front). The results, shown in figure 10 for ϕ = 10 .. 80° indicate that the largest resistance to crack extension occurs near the free surfaces, viz. for ϕ = 10 and 80°, with the latter (corresponding to the TS direction) being the largest. For intermediate ϕ-values, the resistance to crack extension decreases due to the higher degree of local plane strain constraint as shown in figure 9. The above effects of orientation with respect to the rolling direction (TS vs. TL) and of the degree of plane strain constraint on the model's J-R curve behaviour were likewise observed for the SENB specimens, cf. figure 3.
In figure 11, a direct comparison is made between the model and specimen data. This figure presents the following information:

* the model resistance curves of figure 10, contained within the shaded band;
* a resistance curve referring to the crack front averaged model data for each of the seven beach marks, and hence representing an average model J-R curve;

* the specimen J_M-R curves of figure 3, with plane sided and side grooved specimens given by the chain-dotted and dashed lines, respectively.

Based on the information of figure 11 (and considering J_M and J as equivalent in a technical sense for the present model geometry, cf. (1)), it can be concluded for the material and geometry under consideration that the model J-R curve data band is in good agreement with the curves obtained from plane sided specimens. This is attributed to the fact that full plane strain constraint was reached nowhere along the model's crack front (figure 9), so that the model's crack tip stress state will be more similar to that of plane sided than of side grooved specimens (reference (1)). From this it follows that side grooved specimens yield markedly conservative results with respect to the actual structural behaviour. The frequently made assumption in support of side grooving, viz. that plane strain constraint is attained at interior points along the (curved) crack front in three-dimensional geometries, should hence be viewed with caution.

CONCLUSIONS AND RECOMMENDATIONS

Based on the results of the experimental/numerical study presented above, the following conclusions can be drawn with respect to the material and geometries under consideration:

* satisfactory agreement between structural and (SENB) specimen crack growth behaviour is observed up to the final experimental crack extension (i.e. $\Delta a < \approx 9$ mm), provided that the effects of crack tip contraint and orientation of the crack with respect to the rolling direction are taken into account;
* J-R curves obtained from side grooved specimens are conservative with respect to the actual model behaviour;
* the results of the finite element analyses using different meshes (viz. a4 and a6) confirm the need for sufficiently fine meshed in the crack areas.

In view of the limitation of the work reported here to one specific case, viz. a uniaxially loaded flat A387 Gr.D steel plate with two quarter elliptical corner cracks emanating from a central hole, extension of the above conclusions to other geometries and materials should be viewed with caution, although they obviously contain implications for more general application. It is therefore recommended that the above validation of the J-based crack growth concept be extended to other materials and to common engineering geometries such as e.g. (surface) flawed plates, cylinders, vessels and nozzles.

Subsequent to its validation, integration of the J-based crack growth concept into fracture control engineering practice will require the availability of elastic-plastic J-solutions for the above three-dimensional geometries. In view of the magnitude of this task it is recommended that it be undertaken in a cooperative effort of manufacturers and owners of pressure components and other highly loaded, high investment steel structures, preferably within an international framework and under the auspices of the regulatory bodies concerned.

SYMBOLS USED

a4, a6	= mesh with 4 and 6 elements along the crack front, respectively
Δa	= crack growth (m)
J	= J-integral (N/m)
J_M	= Ernst's (3) modified J-integral (N/m)
TL, TS	= crack orientation with respect to the rolling direction
ν_c	= constraint factor
$\sigma_x', \sigma_y', \sigma_z'$	= local tensile stresses (N/m^2)
ϕ	= angular coordinate along the crack front

REFERENCES

(1) Steenkamp, P.A.J.M., "Investigation into the Validity of J-Based Methods for the Prediction of Ductile Tearing and Fracture", Delft University of Technology, Delft, The Netherlands, Ph.D. Thesis, Report WTHD 180, 1986.

(2) Steenkamp, P.A.J.M. and Hartevelt, M., Int. J. Fracture, Vol. 27, pp. R93/R98, 1985.

(3) Ernst, H.A., ASTM-STP 803, Vol. I, pp. I-191/I-213, 1983.

(4) Bakker, A., "The Three-Dimensional J-Integral: An Investigation into its Use for Post-Yield Fracture Safety Assessment", Delft University of Technology, Delft, The Netherlands, Ph.D. Thesis, Report WTHD 167, 1984.

(5) DeLorenzi, H.G. and Shih, C.F., Int. J. Fracture, Vol. 21, pp. 195/220, 1983.

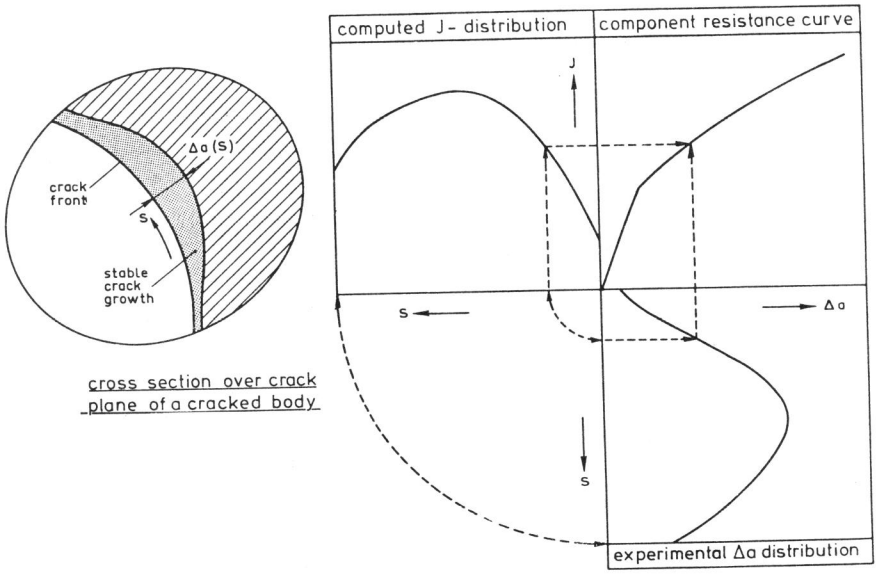

Figure 1 Procedure for determining the J-R curve of a structural geometry

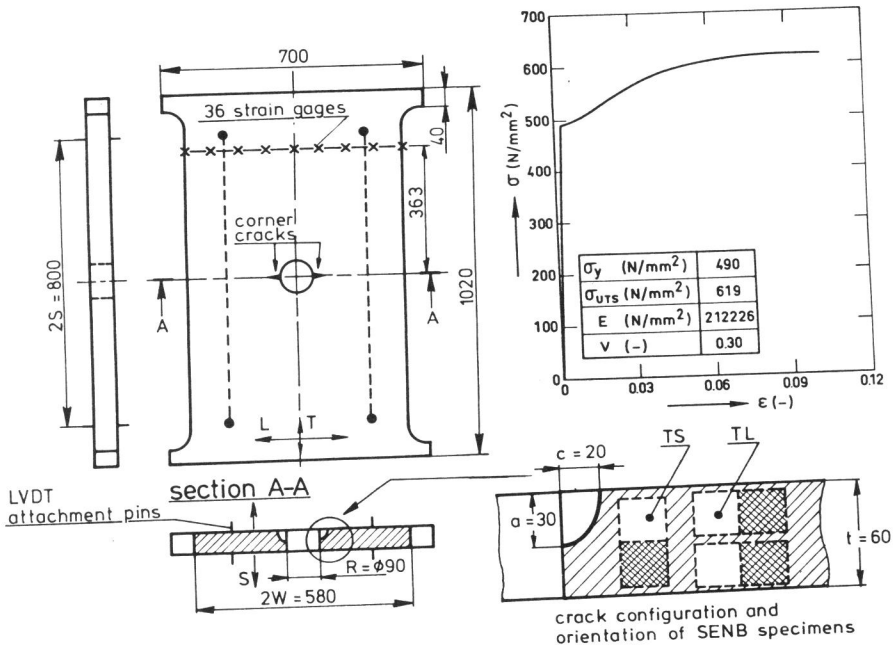

Figure 2 Plate model with central hole and two quarter elliptical corner cracks. T and S indicate the specimen's orientation with respect to the rolling direction L. Insert: engineering stress-strain data

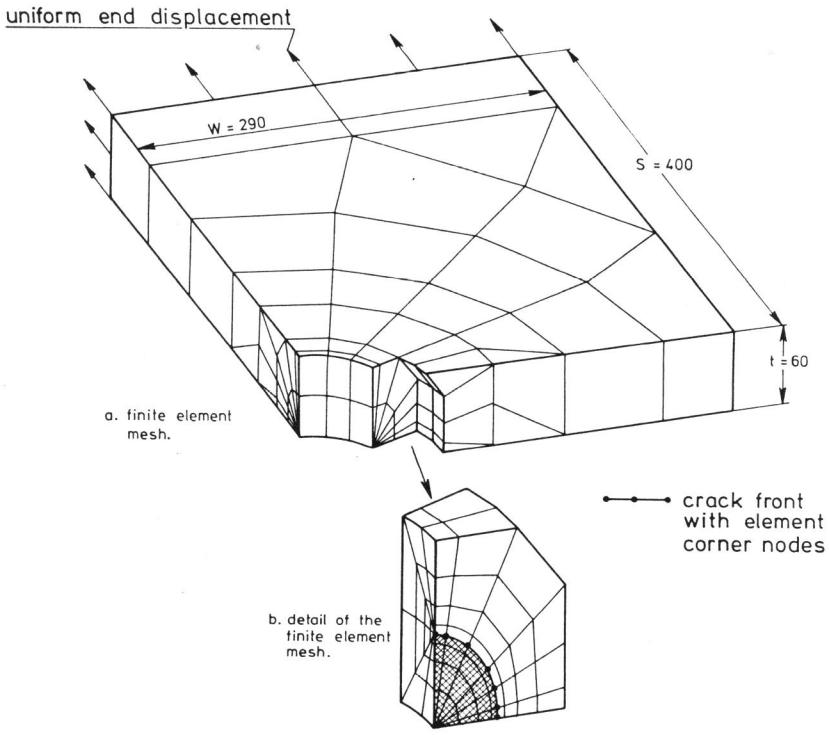

Figure 5 Finite element mesh (a6) for the plate model geometry

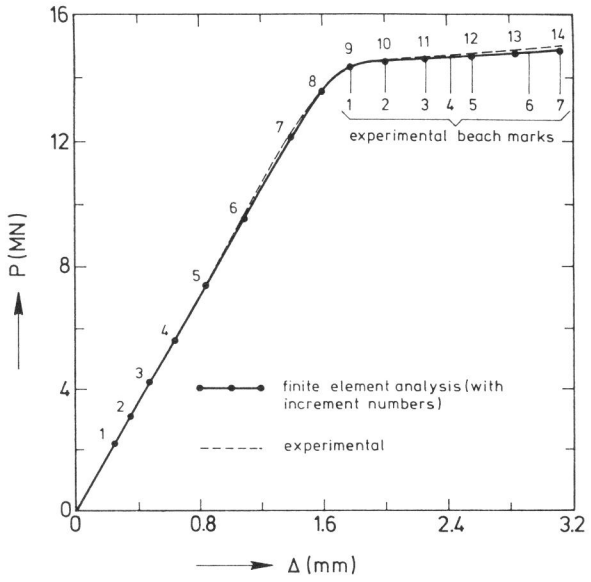

Figure 6 Comparison between experimental and computed load-displacement behaviour of the plate models

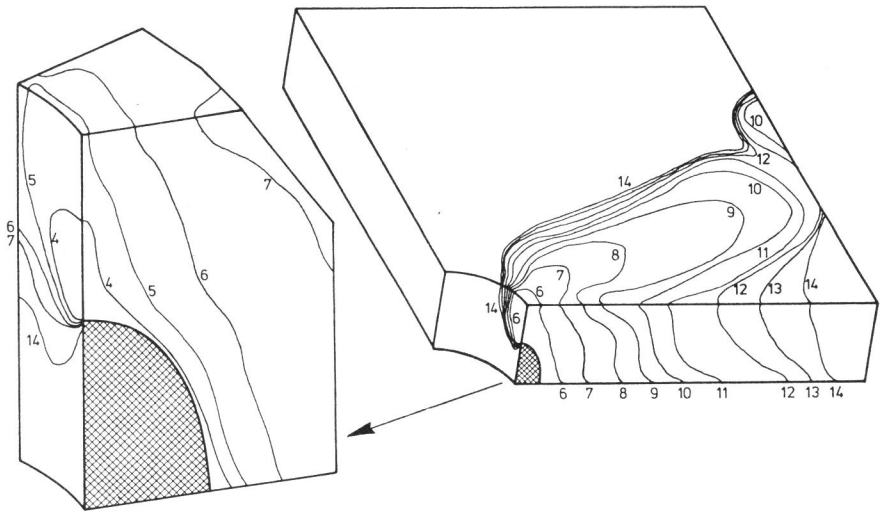

Figure 7 Spreading of the plastic zone in the plate model with increasing load.

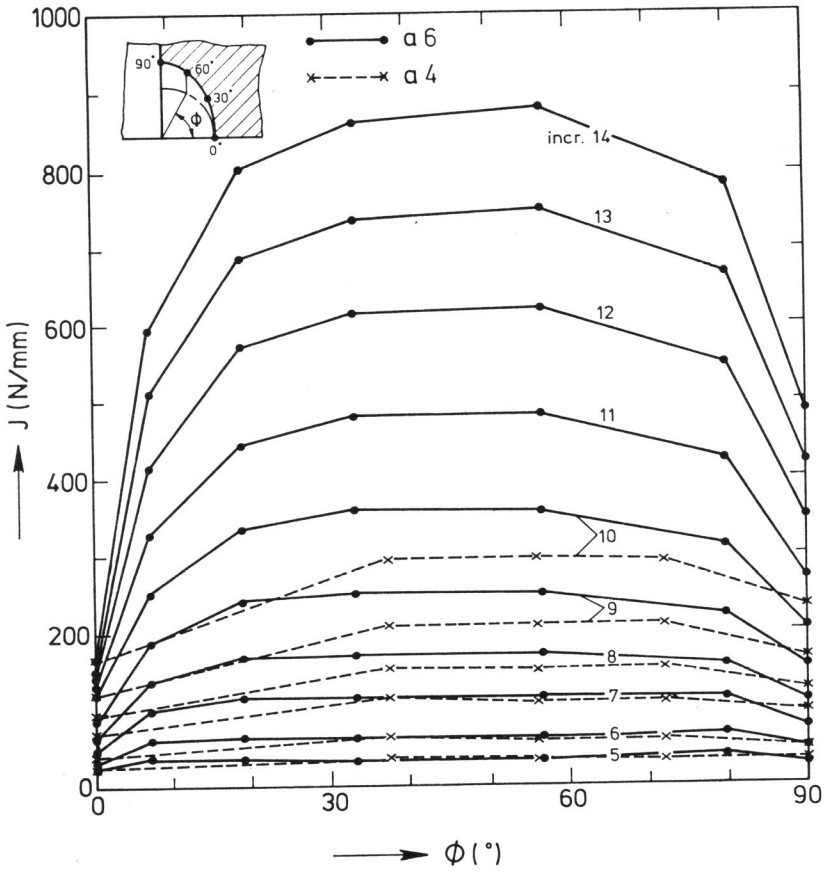

Figure 8 Elastic-plastic J-distributions along the crack front for increasing displacement levels, coinciding with the displacements in figure 6

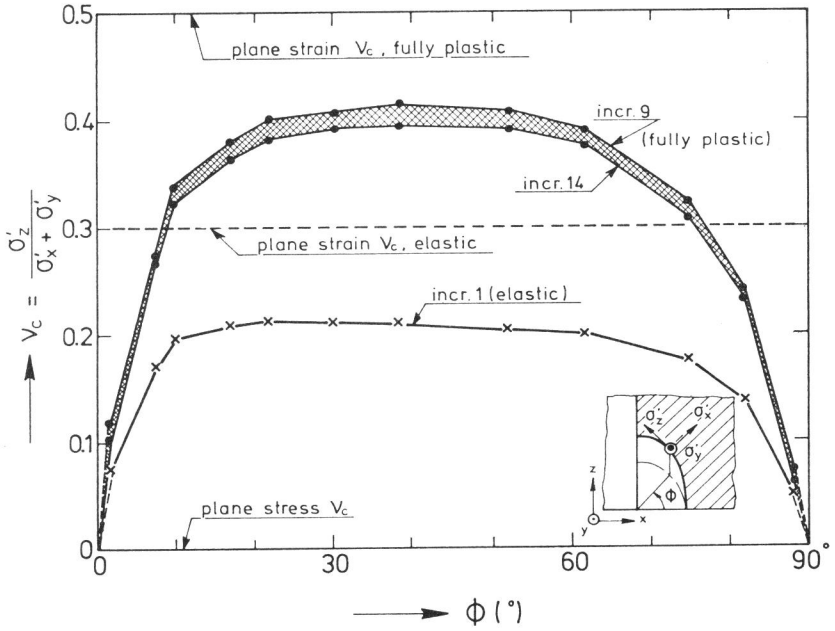

Figure 9 Distribution of the constraint factor along the crack front. Finite element data obtained from a6 analysis

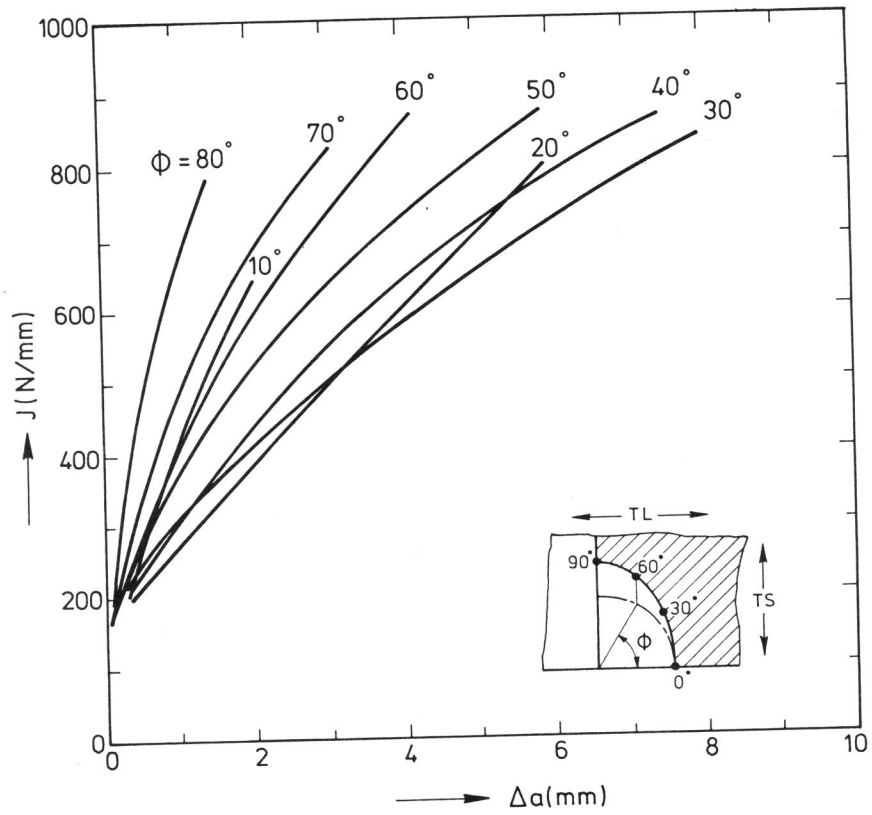

Figure 10 Compilation of local J-R curves for the plate models

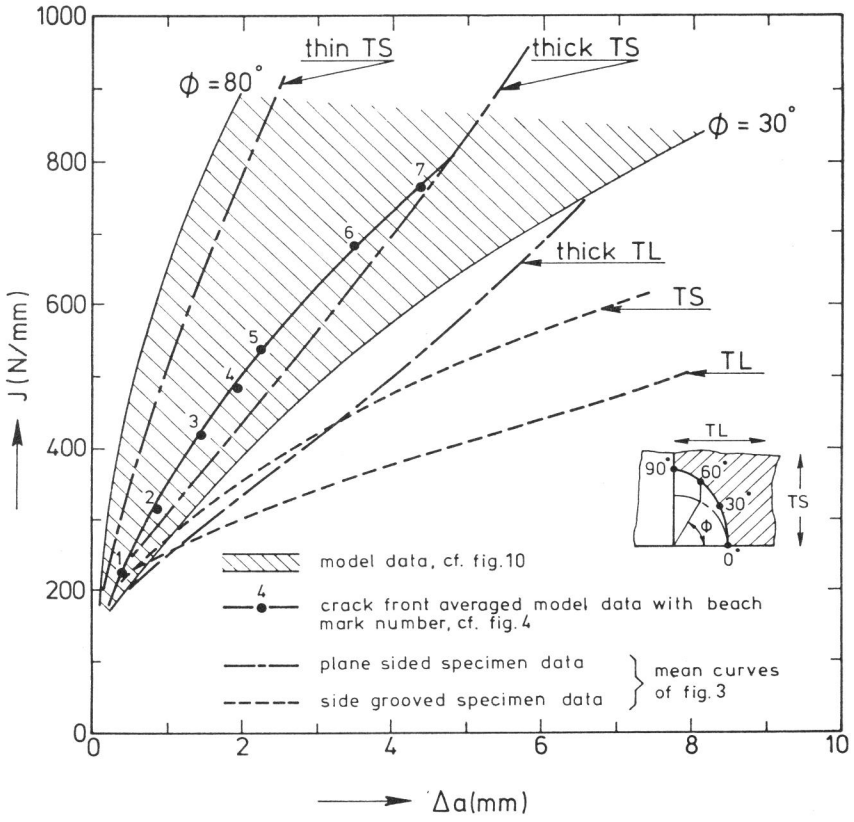

Figure 11 Comparison between model and specimen J-R curves